

# The X-ray Characteristics of a Classical Gamma-Ray Burst and its Afterglow

A. Connors

ISEOS, University of New Hampshire, Durham, NH 03824

and

Geoffrey J. Hueter<sup>1</sup>

Center for Astrophysics and Space Sciences, University of California, San Diego

## ABSTRACT

The serendipitous observation of GRB 780506 by co-aligned  $\gamma$ -ray (*HEAO 1 A-4* 0.02 – 6 MeV) and X-ray (*HEAO 1 A-2* 2–60 keV) instruments during a six hr pointing at a blank section of the sky gave us unprecedented high signal-to-noise X-ray spectra and light curves of a  $\gamma$ -ray burst and its afterglow. First, the spectra: although the time resolution was only 10.24 s, it was possible to derive unambiguous position constraints and a reliable instrument response. We therefore could see two breaks in the initial spectrum, one consistent with a peak in  $\nu F_\nu$  of  $\sim 45$  keV, and one below 4 keV, consistent with strong absorption. The event exhibited dramatic spectral variability, hardening as it rose to each peak, and softening as it fell, similar to behavior reported above 100 keV from other bursts. The initial strong turnover below a few keV evolved into a slight excess as the burst progressed. The spectral shape varied widely outside low energy limits prescribed by current relativistic shock models. At no time was there evidence for any lines, either in emission or absorption. Overall,  $\sim 20\%$  of the total energy was radiated in nonthermal 2–30 keV X-rays. Second, the light curve: the X-ray proportional counters were able to monitor the flux for an hour before and some hours after burst onset. Two minutes after it ended, *HEAO 1 A-2* detected a faint resurgence of 2–10 keV flux, rising to a peak  $\sim$ seven minutes after burst onset, followed by irregular emission with best-fit decay time of  $\sim \frac{1}{2}$  hr. The position of the source of the extended flux is consistent with that of the burst, and probably not from a serendipitous transient. We estimated that the entire afterglow radiated between 3 and 30% of the  $>1$  keV energy radiated during the burst. In this paper, we present the 2–300 keV *HEAO 1 A-2* and A-4 light curves and spectra from GRB 780506, and its apparent  $\sim 1$  keV afterglow.

*Subject headings:* X-rays: general — gamma-rays: bursts — methods: statistical

---

<sup>1</sup>Now at Far Point Technology, P.O. Box 421467, San Diego CA 92142

## 1. Introduction

We present a serendipitous observation of 2–300 keV X-rays from a “classic”  $\gamma$ -ray burst, GRB 780506, observed on May 6, 1978, during a  $\sim 6$  hr pointed maneuver. The event was discovered in *HEAO 1* A–4 (0.03–6 MeV) data (Hueter 1987), and subsequently found to have been detected by *HEAO 1* A–2 (2–60 keV). The detectors observed the same region of sky for about  $1\frac{1}{2}$  hr before and  $4\frac{1}{2}$  hr after the event. We obtained complete coverage of the  $\gamma$ -ray burst with instruments spanning three decades in energy; and reasonably continuous coverage (the source was eclipsed by the Earth about 30% of the time) of the associated fainter longer time-scale emission, which we had termed the afterglow. (See Connors and McConnell 1996 for a preliminary report.) Although the event was faint at higher energies, ( $\sim 7 \times 10^{-7}$  ergs-cm $^{-2}$  0.03–6 MeV), below 60 keV the small field of view, low background, good position constraints, and  $\sim 400$  cm $^2$  effective area combined to give high signal-to-noise data down to 2 keV. We obtained good signal-to-noise 2–60 keV spectra every 10.24 s, with well-characterized instrument response. This is a rare combination.

Until the launch of the wide field of view *Ginga* satellite, out of hundreds of  $\gamma$ -ray bursts,  $<10$  keV X-rays had been detected from only a handful (Wheaton et al. 1973; Cline et al. 1979; Gilman et al. 1980; Terrell et al. 1982; Laros et al. 1984a,b; Katoh et al. 1984). These earliest measurements of  $<10$  keV X-rays from  $\gamma$ -ray bursts suffered from small collecting areas ( $\sim$ several cm $^2$ ) and ill-constrained positions (Wheaton et al. 1973; Gilman et al. 1980). Many were limited to data from scanning instruments, so that  $<10$  keV light curves were sampled in snapshots at regular intervals; or did not have continuous spectral coverage from  $\gamma$ -rays down to X-rays (Laros et al. 1984a,b, Katoh et al. 1984; Terrell et al. 1982). In the past decade, the large field of view  $\gamma$ -ray burst detectors, on board the Japanese satellite *Ginga*, have been able to measure X-rays from a significant sample, observing both line features (Murakami et al. 1988; Fenimore et al. 1988; Yoshida et al. 1992; Graziani et al. 1992), and continuum characteristics (Strohmayr et al. 1998). They observe a variety of  $<20$  keV spectral shapes, from flattening and occasional rollovers at a few keV, to continued increases in roughly half their events. However large field of view instruments can bring with them problems of high background and poorly constrained positions. For *Ginga*, below  $\sim 10$  keV, the spectra were uncertain by 30% due to unknown incidence angles in all but four of the events. Also, the higher background inherent in a low spatial-resolution X-ray instrument could preclude detecting any extended afterglow unless it were exceptionally bright.

Recently, arc-minute localizations of nine bright  $\gamma$ -ray bursts have been made available hours after burst onset, due to the Italian–Dutch *BeppoSAX* satellite (Heise et al. 1997,1998; Piro et al. 1997,1998a,b; Costa et al. 1997,1998; Halpern et al. 1997); *RXTE*’s All-Sky Monitor (Smith et al. 1998); and coordinated efforts among *CGRO* and scans by *RXTE*’s PCA (Takeshima et al. 1998 and references therein). This has allowed more sensitive, small field of view instruments to be repointed to search for X-ray and longer-wavelength afterglows (for example Murakami et al. 1998). In at least seven of the nine recent well-localized events, faint ( $< \text{few} \times 10^{-12}$  ergs-cm $^{-2}$ -s $^{-1}$ ) fading afterglows were detected, typically hours or days later.

By contrast, in these *HEAO 1* data we observe the burst position directly after the event, allowing detection of the initial resurgence in soft X-ray flux. For this event, one sees this soft emission peak about seven minutes after burst onset, or about five minutes after flux from the initial event has returned to background.

The burst itself was softer than average, with a power-law photon index of  $-2.4$  above  $\sim 45$  keV, implying it may be a representative of a soft subset of  $\gamma$ -ray burst emission (Pizzichini 1995; Kouveliotou et al. 1996; Belli 1997; Pendleton et al. 1997). Nevertheless, many of the features observed in GRB 780506 were also visible, with less statistical significance, in the earlier measurements of X-rays from  $\gamma$ -ray bursts. The soft X-rays in general lasted longer than the higher energy emission; the event exhibited rapid spectral variability, hardening as it rose to each peak and softening as it fell; and there was a dearth of soft photons just prior to the first peak. This continues a pattern often noted in other bursts at higher energies: the shape of the light curve at lower energy, in general, follows that of the slightly higher energies, but with a slight soft lag, and with a ‘smearing’ of the softer emission; and the emission softening from peak to peak (Norris et al. 1986; Band et al. 1992; 1993; Ford et al. 1994; Kargatis et al. 1994). Other observations have suggested these effects become more pronounced below about 50 keV. (For example see GRB 830801 in Laros and Nishimura 1986.) Also, despite this event’s relatively soft spectrum, the X-ray spectra were too flat to be fit by any simple thermal model. The  $<50$  keV spectral shape evolved from a flat power-law (photon index  $-1.1$ ) with significant absorption below a few keV, to a steeper power-law with an increasing (but still small) amount of excess emission below a few keV that could be modeled by a black-body component. In particular,  $<10\%$  could have been attributed to cooling black-body emission from reprocessing in optically thick material. This suggests to us that the bulk of X-rays were generated through the same non-thermal processes driving the  $\gamma$ -ray spectral evolution, rather than deriving from a separate thermal component, in contrast to the conclusions of Laros and Nishimura (1986) and Cherenko and Mitrofanov (1994).

In the following section we describe the instrument, present the GRB 780506 light-curves and spectra, and compare them with other observations of X-rays from  $\gamma$ -ray bursts. We conclude with a brief summary in Section 3. (Appendix A details the Bayesian algorithms used to determine the burst and afterglow positions.)

## 2. Observations and Analysis

### 2.1. The Experiments

The *HEAO 1* satellite observed the sky from August 1977 to January 1979 with four different sky survey experiments (A-1, A-2, A-3, and A-4) spanning the energy range 0.1 keV – 6 MeV. Only the two widest field-of-view instruments, A-4 (0.03 – 10 MeV) and A-2 (0.1 – 60 keV), detected GRB 780506. The A-4 experiment consisted of three sets of sodium iodide/cesium iodide phoswich detectors (A-4 HED, 0.1–6 MeV  $40^\circ$  FWHM circular field of view; four A-4 MEDs,

0.03–3 MeV,  $16^\circ$  FWHM circular fields of view; and two A–4 LEDs, 10–200 keV,  $1.7^\circ \times 20^\circ$  collimated slats; Matteson 1978). The six A–2 multiwire, multilayer proportional counters were designed with overlapping medium and small fields of view — both within each detector and among detectors — for stable and well-monitored internal and cosmic background (Rothschild et al. 1979). We used these to constrain the position of the burst and afterglow. The A–2 HED1 (xenon plus propane veto layer, 2–60 keV,  $3^\circ \times 6^\circ$  plus  $3^\circ \times 3^\circ$ ) look-direction was offset by  $6^\circ$  from the others (A–2 MED, argon plus propane veto layer, 1–20 keV,  $3^\circ \times 1.5^\circ$  plus  $3^\circ \times 3^\circ$ ; A–2 HED2, xenon, 1–60 keV,  $3^\circ \times 6^\circ$  plus  $3^\circ \times 3^\circ$ ; and A–2 HED3, xenon plus propane veto layer, 2–60 keV,  $3^\circ \times 1.5^\circ$  plus  $3^\circ \times 3^\circ$ ). The A–2 LEDs were turned off at this time. GRB 780506 was detected only in the A–4 MEDs and the offset A–2 HED1 detector.

## 2.2. Burst detection

The authors had independently performed statistical surveys of all the *HEAO 1* A–4 data (10 keV–6 MeV; Hueter 1987) and the “scanning” portion of the *HEAO 1* A–2 data (2–60 keV; Connors 1988; Connors, Serlemitsos, and Swank 1986), for events with durations comparable to those of  $\gamma$ -ray bursts. Out of 21  $\gamma$ -ray bursts uncovered in the A–4 survey, only two were found in A–2 data with greater than  $\sim 3\sigma$  significance. The stronger of the two, found in A–2 scanning data, was detected through the sides of the A–2 detectors and so was not useful for observing  $< 50$  keV X-rays (Connors 1988). The fainter of the two was found to have occurred during a  $\sim 6.5$  hr pointed maneuver, in a region of sky containing no previously known X-ray sources. (Pointed data were not covered by the A–2 systematic survey of Connors 1988). This event, occurring on May 6, 1978 and given the designation GRB 780506, was the only  $\gamma$ -ray burst observed through the aperture of an A–2 detector (rather than through the sides). Since the A–2 fields of view were roughly twenty times smaller than the A–4 MED fields of view, this is about the rate of A–2 detections one expects

Hueter (1987) classified GRB 780506 as a faint (fluence  $\sim 7 \times 10^{-7}$  ergs-cm $^{-2}$  0.03–6 MeV)  $\gamma$ -ray burst, with duration  $\sim 10$  s, and a photon power law spectral index (above 30 keV) of  $2.4 \pm 0.3$ . It was observed with three of the A–4 MEDs (the fourth was covered by the blocking crystal), with energy ranges 25–100 keV, 70–1900 keV, and 100–2900 keV. The event was not detected in either of the two A–4 LEDs, indicating that the burst position was outside their fields of view. On the basis of its moderate duration, reasonably hard spectrum, and spectral variability, we classified this event as a classic  $\gamma$ -ray burst, rather than a soft  $\gamma$ -ray repeater (Norris et al. 1991). In BATSE data it would have been classified as a member of the longer subset of  $\gamma$ -ray bursts (Kouveliotou et al. 1994).

In contrast to the rates from the A–2 HED1 offset xenon proportional counter, which rose from a background rate of  $\sim 20$  cts-s $^{-1}$  to over 500 cts-s $^{-1}$ , the rates from A–2 HED3, an identical xenon proportional counter with a slightly different look direction and field of view, rose from 15 cts-s $^{-1}$  to 16 cts-s $^{-1}$  during the 10 s interval flagged by A–4 data as GRB 780506. Therefore we

concluded that A–2 HED1 had detected X–rays through the front of its collimators, rather than  $\gamma$ –rays or charged particles through its sides.

The burst occurred while the orientation of the satellite was held fixed so that the A–1 instruments on the opposite side of the spacecraft could point at the bright X–ray binary Cygnus X–1. During this maneuver, the A–2 and A–4 experiments viewed a “blank” section of the sky near the Galactic plane. They viewed this same section of sky three and six days after GRB 780506 as the A–1 experiment pointed at Cygnus X–1 several times. Each “blank sky point” lasted for roughly 6 hr, interrupted by 20–30 minutes of Earth eclipse every  $\sim 90$  minute orbit. The *HEAO 1* experiments also scanned this region for several days before and after the event, viewing the region for  $\sim 1$  minute every 35 minutes.

In Figure 1 we present the A–2 HED1 Layer 1 2–20 keV light curve, plotted in 122.88 s bins. We subtracted a mean background rate determined from the first hour of the blank sky point. (The small bump visible in the first orbit is not significant, as  $\chi^2$  for a fit to a constant rate was 14. for 17 122.88 s bins, or 354. for 362 5.12 s bins.) To reduce times of high particle background, we have excluded times with MacIlwain’s  $L$ –parameter  $> 1.4$  (equivalent to times of low rigidity; Tennant 1983). The burst itself is contained in the single highest  $\sim 2$  minute bin, visible shortly after the second gap (due to Earth occultation). One then observes a slow resurgence of 2–20 keV flux. For A–2 HED1,  $\chi^2$  for a fit to a constant, zero, rate was 72.6 for 21 122.88 s bins; or  $\chi^2$  of 531. for 440 5.12 s bins, for the remainder of the orbit following the burst. The count rate was constant in the 2–20 keV energy band of the A–2 HED3 (identical to A–2 HED1 save for look direction and field of view) during this same time period ( $\chi^2$  of 13.8 per 21 122.88 s bins; or  $\chi^2$  of 417. for 440 5.12 s bins for a fit to a constant zero rate), indicating again that the increased counts came from X–rays from the source rather than charged particles or  $\gamma$ –rays through the detector walls. Also, the spectra of the high–flux points after the burst (including those in the second half of that orbit) were quite soft, while instrumental background has quite a hard spectrum.

Given the position error–box (see below), and rates of serendipitous X–ray sources (Connors et al. 1986, Motch et al. 1991a,b; Linsky 1990), Connors and McConnell (1996) calculated a  $> 98.5\%$  probability that the longer–duration emission came from the same source as the burst. Additionally, using ROSAT data they searched for a serendipitous X–ray transient that could have produced one or both, with null result. We therefore had associated this soft, slowly varying emission with the burster, and had termed it the afterglow (Connors and McConnell 1995,1996; Connors 1988).

### 2.3. Position Constraints

Only the A–2 offset detector, HED1, showed a significant increase in counts at the time of the burst, constraining the source to be more distant than  $-6^\circ$  (along the satellite spin–direction) from the main detector axis. To further constrain the source position, we used a Bayesian

algorithm that compared the measured rates in the overlapping wide and narrow fields of view, every 5.12 s, against a model position, background rates, and intensity in that time bin (Appendix A). The orbit preceding the burst was used to estimate the prior probability of the background rates (see Figure 1). This was done separately for the burst itself and the extended emission following the burst (Appendix A). For GRB 780506, we calculated the best fit position to be at 2000.0 R.A. and Dec.  $\sim 7^h 42^m 48^s$ ,  $-41^\circ 51' 18''$  or Galactic  $l^{II}, b^{II}$  of  $255.6^\circ, -9.0^\circ$ , with  $3\sigma$  (99.73%) credible limits of  $\pm 0.16^\circ$  along the satellite spin direction, and  $\pm 3^\circ$  perpendicular to it. Although not exactly a quadrilateral, the corners of this A-2  $3\sigma$  credible region were roughly  $118.9^\circ, -42.73^\circ$ ;  $112.5^\circ, -40.56^\circ$ ;  $118.9^\circ, -43.04^\circ$ ; and  $112.5^\circ, -40.87^\circ$  (2000.0 R.A. and Dec). For the extended emission, the  $3\sigma$  contours were approximately centered on those of GRB 780506, with a width of  $\sim \pm 0.5^\circ$ . The corners of its A-2  $3\sigma$  credible region were roughly  $118.8^\circ, -42.36^\circ$ ;  $113.2^\circ, -40.50^\circ$ ;  $118.3^\circ, -43.31^\circ$ ; and  $112.7^\circ, -41.43^\circ$  (2000.0 R.A. and Dec).

To further constrain the source position in the direction perpendicular to the satellite spin plane, we compared rates from A-2 HED1 and the much wider field of view A-4 MEDs, in the  $\sim 30$ – $60$  keV range that their spectral windows overlapped. We first calculated the incident A-2 and A-4 photons-cm $^{-2}$ -s $^{-1}$  in the four overlapping energy channels, assuming the best-fit spectrum discussed in §2.6. (Since the GRB 780506 spectra were relatively smooth and featureless, our results were insensitive to the specific model employed, as long as the fits were reasonably good.) A least  $\chi^2$  fit minimizing the differences in incident A-2/A-4 photon flux in 4 channels in the 30-60 keV region of overlap, during the first, brightest, 10.24 s of the burst, showed the source position to lie  $\pm 1^\circ$  (with a  $1\sigma$  uncertainty of  $0.5^\circ$ ) from the satellite spin plane, with A-2/A-4 best fit positions of  $116.9^\circ, -42.26^\circ$ ; and  $114.5^\circ, -41.42^\circ$  (2000.0 R.A. and Dec.), or about  $7.3^\circ$  off the main detector axis. The  $\gamma$ -ray burster was located outside the A-3 field of view; and although it appeared to be on the edge of one module of the A-1 field of view, exceptionally high background rates at the time of the burst precluded using the A-1 rates to further constrain the position (J. Norris 1988, private communication). For the A-2 burst light-curves (Figure 2) and spectral analysis (Figures 3 and 4), we arbitrarily assumed one of the two best fit positions given above ( $114.5^\circ, -41.42^\circ$  2000.0 R.A. and Dec.), although this choice makes little difference to the instrument response.

#### 2.4. Burst Light Curves and Hardness Ratios

In Figure 2, we present the A-2 and A-4 light-curves during just the single highest 122.8 s time bin of Figure 1. We used time bins of 1.28 s, which was the shortest integration time available from the A-2 HED1 during this observation. At the top we have plotted the A-4 count-rates for A-4 MED1 (90–2900 keV) and all A-4 MEDs below 200 keV (25–200 keV) for this event. Directly below are the 8–45 keV light curve from A-2 HED1 and the 2–6 keV light curve from the same instrument. At the bottom, we have displayed the 8–45 keV/2–6 keV hardness ratio. (The event was too faint for us to form meaningful hardness ratios  $>100$  keV.) Several features hinted at in

earlier reports of X-ray counterparts are immediately apparent. Overall, the event softens as it progresses. The emission hardened as it rose to each peak, and softened as it fell. A second main peak, which was not visible in the  $>30$  keV light curves, was apparent in the 8–40 keV band. In the 2–6 keV X-rays, it was brighter than the first main peak. The longer wavelengths appear to have a longer decay time than the shorter wavelengths, and although emission at all wavelengths appears to begin to rise at the same time, the softer light curve appears to peak on the order of 1 s after the harder ones. This is consistent with what was observed for many (but not all) *Ginga* bursts (Strohmayer et al. 1998; Murakami et al. 1992; Yoshida et al. 1989).

At higher energies, the evolution of different energy light-curves has been described in two parts: an increasing width of each peak as energy decreases; and a soft lag. Using BATSE data, Fenimore et al. (1995) have parametrized the average peak width as a function of energy with a power-law,  $W_{ac}(E) = 17.43E^{-0.43}$ ; where  $W_{ac}(E)$  is the width (in seconds) of an average autocorrelation function at energy  $E$ , measured where the value of the average autocorrelation is at  $e^{-\frac{1}{2}}$  the value at its peak. We compare this with the width of two peaks measured at 2–6 keV and 8–45 keV, in Figure 2. Rather than taking the autocorrelation, we simply measure the width of each pulse at  $e^{-\frac{1}{2}}$  of the peak value. For the first peak, one finds widths of  $\sim 7 \pm 1$  s and  $\sim 10 \pm 1$  s at 8–45 keV and 2–6 keV, respectively. For the second peak, one measures  $\sim 8 \pm 1$  s and  $\sim 12 \pm 1$  s, for the same energies. (This second peak was not detected in the A-4  $> 25$  keV data.) Fenimore et al. (1995) point out the widths in each energy band will be dominated by the timescale of the lowest energy in each. Using their formula to extrapolate to X-ray energies, one predicts timescales of  $\sim 7.1$  s and 13 s, at 8 keV and 2 keV, respectively; in agreement with the values measured from GRB 780506. That is, the same mechanism appears to drive the widths of the pulses from a few hundred keV down to  $\sim 2$  keV. We suggest that it is this soft lag and longer decay time that could have been interpreted, when incompletely sampled or when continuous spectral coverage was not available in earlier measurements, as a soft, thermal, component which varied independently of the  $> 30$  keV  $\gamma$ -rays (Laros and Nishimura 1986).

Although a lag of the peak of softer energies with respect to harder ones has often been noted at higher energies, (Chernenko et al. 1998; Chipman 1994; Band et al. 1992; Norris et al. 1986), it is not as well quantified as a function of energy. It may be related to an evolving low energy cut-off seen both here, in GRB 780506; and at higher energies (Pendleton et al. 1996).

Vietri (1997), discussing the rather similar light-curve of GRB 970228, attributes the second peak to an afterglow due to a reverse (external) shock. However we note: 1) under that definition, even longer BATSE bursts with multiple, widely separated peaks — such as the well-known bright burst GRB 910503, BATSE trigger 143 — would have been classified as having afterglows; 2) when the 2–60 keV X-ray spectra are looked at in detail, no evidence for a different kind of emission in the second peak is apparent; and 3) the wide variety of burst light-curves seen both at wavelengths  $> 20$  keV (Fishman, J.G. et al. 1994) and below (see references in Katoh et al. 1984; Laros et al. 1984a; Laros and Nishimura 1986; Murakami et al. 1988, 1991; and Strohmayer et al. 1998); caution against making such an identification from one or two bursts.

## 2.5. Burst Spectra

At the time of the burst, pulse height analyzed data were read out every 10.24 s for A–2 HED1, and every 5.12 s for the A–4 detectors. We have marked the 10.24 s accumulation intervals at the top of Figure 2 as intervals 1 through 6. The A–4 instruments detected the burst only in the first 10.24 s, which contained the rise and fall of the first peak. In Figure 3, we display the  $\nu F_\nu$  spectrum of the first peak (intervals 1 and 2); second peak (intervals 3, 4, and 5); and the 600 s of the afterglow during which it was brightest. The photon–fluence and error bars of each point were determined from the best–fit model, by scaling the observed counts and errors by the ratio of the model to the predicted counts in each channel. These were multiplied by the average energy in each bin to obtain  $\nu F_\nu$  spectra. The A–2 and A–4 data were fit separately. The A–4 data were well–fit by a simple power–law. For the A–2  $< 60$  keV spectra, the only model that fit not only the hard emission above 10 keV, but also the initial strong low–energy turnover and the growing soft excess below  $\sim 6$  keV was a superposition of a power law plus a black body, of the form

$$\frac{dN}{dE} = \left( A_1 \frac{E^2}{\exp(E/kT) - 1} + A_2 E^{-\alpha} \right) e^{-\sigma_{abs} N_H} \quad (1)$$

where  $\sigma_{abs} N_H$  is the amount of photoelectric absorption of a hydrogen column density  $N_H$  at energy  $E$  (assuming Galactic abundances). (Other models we tried that did not fit included linear combinations of power–laws, thermal bremsstrahlung, and thermal synchrotron spectra. The frequently used “GRB” function of Band et al. 1993 does not model an upturning spectrum and so was not a good representation of the evolving  $< 20$  keV spectra.) We emphasize that these were only empirical fits, to illustrate the overall shape of the spectrum in each interval.

Overall, we consider the X–ray to  $\gamma$ –ray spectra of  $\gamma$ –ray bursts to consist of four parts: 1) the highest energy emission, which can extend in a power–law above a break energy beyond tens of MeV to GeV energies (Kippen et al. 1998; Dingus et al. 1994; Matz et al. 1985); 2) the intermediate energy emission, which tends to roll over to a peak in  $\nu F_\nu$  typically at  $\sim 200$  keV (but with a wide spread; Band et al. 1993; Kargatis et al. 1994); 3) the X–ray spectrum below 30–50 keV, which can either continue or flatten even more (Laros et al. 1984a,b; Strohmayer et al. 1998); and 4) a lower energy turnover, or flattening, or sometimes excess below several keV (Strohmayer et al. 1998; Katoh et al. 1984; Preece et al. 1996), consistent with heavy intrinsic absorption, or excess thermal emission, respectively. One also typically (but not universally) observes a softening trend in successive peaks (Norris et al. 1986; Ford et al. 1994; Band et al. 1992).

From Figure 3, one sees GRB 780506 to have followed these patterns. The bulk of the emission was emitted in the first peak. The  $> 50$  keV  $\gamma$ –rays of exhibited a steeper than average spectrum with a photon power law index of about  $2.4 \pm 0.3$ . For all bursts in Hueter (1987) the mean was  $1.6 \pm 0.05$ . This places GRB 780506 in the ‘soft’ subclass of  $\gamma$ –ray bursts suggested by Pizzichini (1995); Belli (1997), with a 100–300 keV / 50–100 keV fluence hardness ratio of  $\sim 1.1$  (while for an  $E^{-1.6}$  spectrum it would be  $\sim 2.3$ ). This subclass shows no evidence for turnover



from a  $\log(N > P) - \log(P)$  distribution of  $P^{-\frac{3}{2}}$  (Belli 1997; Kouveliotou et al. 1996; Pizzichini 1995; Pendleton et al. 1997). For the first peak, the maximum in  $\nu F_\nu$  occurred around 45 keV where the A-2 and A-4 data overlap. Below this the *HEAO 1* A-2 spectrum of the first peak is consistent with a power law with photon index  $1.17 \pm 0.01$ . There is an indication of a low energy turnover equivalent to an absorption of  $0.1 \pm 0.04 \times 10^{23} \text{ cm}^{-2}$ .

In these data, the distinction between the medium-energy turnover ( $\sim 45 \text{ keV}$ ) and low-energy turnover (a few keV) is explicit. This is not always the case in *Ginga* data (Strohmayer et al. 1998).

For the second peak, there is no significant A-4 emission and the data are too uncertain to constrain a maximum in  $\nu F_\nu$ . The A-2 emission is softer (photon index  $1.8 \pm 0.01$ ) and, instead of a turnover at low energies, shows emission slightly in excess of the power law. This we fit with a black-body spectrum with temperature  $1.8 \pm 0.06 \text{ keV}$ .

The spectrum of the afterglow was not well-constrained. We found a  $1.1 \pm 0.4 \text{ keV}$  black body with negligible absorption, a  $2.4_{-0.8}^{+1.3} \text{ keV}$  thin thermal bremsstrahlung model, and a heavily absorbed, power law spectrum with photon index of  $3.9_{-0.8}^{+1.8}$  all fit equally well. (A power law with photon index  $2.8 \pm 0.1$ , with the absorption fixed at zero, was also acceptable.) We saw no evidence of hardening or softening during the afterglow.

However it is clear from Figure 2 that we have integrated over dramatic spectral variations. Therefore in Figure 4.a-4.f we display the spectra on shorter (10.24 s) timescales. These we plotted in  $\text{photons-cm}^{-2}\text{-s}^{-1}\text{-keV}^{-1}$  to better reveal the low energy turnover evolving to a slight excess; and for detailed comparisons with other published X-ray spectra. Following Strohmayer et al. 1998, in Figure 4.g we plot the best-fit model spectra but normalized to unity at 10 keV, to better illustrate the evolution of just the spectral shape. Notice the fraction of low energy emission consistently rises as the burst progresses. We list the parameters from empirical fits to these data in Table 1. At no time was there evidence for a line feature, either in emission or absorption. For all the spectra, adding a line described by three parameters (width, intensity, and line energy) reduced the value of  $\chi^2$  by less than 3; and adding a line described by two parameters (width and intensity, with the energy fixed at that of one of the *Ginga*/LANL lines; Murakami et al. 1988; Fenimore et al. 1988) lowered  $\chi^2$  by less than 2.

The first spectrum contains the rise and maximum of the first peak. Using just an absorbed power-law model, one finds it is very flat (photon index  $1.10 \pm 0.4$  from 2-50 keV), and featureless out to a slight apparent steepening of the spectrum that starts at around 45 keV. This is too flat to accommodate a thermal synchrotron model, or even a sum of hardening thin thermal bremsstrahlung spectra, or of black body spectra. The turnover at low energies is most pronounced, consistent with a high average absorption of  $0.3 \pm 0.05 \times 10^{23} \text{ cm}^{-2}$  (estimated using the power-law model with no black-body component). This is greater, by over an order of magnitude, than the total interstellar column density to the edge of the Galaxy in this direction (Lucke 1978; Kerr et al. 1986; Lang 1980). This low energy turnover is not present in any of the spectra from later

time intervals, including the second peak. All show column densities consistent with zero, and in fact show evidence for a slight excess above the power-law.

If one scrutinizes the  $<5$  keV spectra from other  $\gamma$ -ray bursts, one notices a similar dearth of low energy photons at the time of the first peak, although this is not always present (Strohmayer et al. 1998; Murakami et al. 1992 and references therein; Katoh et al. 1984). We note this is consistent with “evolving low energy cutoffs” observed at higher energies on the rising edge of some peaks of other  $\gamma$ -ray bursts (Strohmayer et al. 1998; Kargatis et al. 1994; and Pendleton et al. 1996). However it is interesting to note that when this low-energy turnover exists in a  $\gamma$ -ray burst, it apparently does not always occur on the rising edge of the first peak. There is a dramatic example in Katoh et al. (1984) of extreme low energy suppression in the middle of a burst.

As each of the two main peaks decays, the high energy tail steepens, while the peak of the emission shifts to lower and lower energies. This “black body” portion of the low energy emission comprises  $\sim 10\%$  of the  $<60$  keV emission and  $\sim 2\%$  of the total emission. For GRB 780506, we estimate the 3–10 keV emission to be  $\sim 6\%$  of the energy emitted  $>30$  keV, during just the first peak of the burst; when we included both peaks of the burst, we found roughly 7–20% of the total burst energy was emitted between 3–10 keV, with the uncertainty due chiefly to the uncertainty in the shape of the spectrum  $>50$  keV as the burst progressed. This is higher than similar ratios calculated for most of the other  $\gamma$ -ray bursts for which it has been measured ( $\sim 1\%$ – $3\%$ , from Laros et al. 1984a,b;  $\sim 0.5\%$ , with an uncertainty of a factor of 5, from Figure 6 of Katoh et al. 1984; and  $\sim 1\%$ – $10\%$  from Table 1 in Strohmayer et al. 1998, for the four bursts with known positions). From comparisons of the spectral shapes, one finds this is due to less  $> 45$  keV emission in GRB 780506 (i.e. steeper than average power-law at higher energies) rather than softer or less highly absorbed low energy emission.

Although Murakami et al. (1988) preferred to interpret the softening spectrum in the decay portion of each peak as cooling black-body emission, in GRB 780506, a power law tail was visible, ruling out both simple superpositions of thermal bremsstrahlung and black body spectra, for as long as there were sufficient counts per energy bin to distinguish among spectral models. This is in fact consistent the *Ginga* X-ray observations (Murakami et al. 1988; Yoshida et al. 1989; Murakami et al. 1992). Earlier measurements of X-ray emission did not have good spectral data below several keV, so comparisons were not feasible.

Imamura and Epstein (1986) and Epstein (1986) pointed out that, even under the assumption that most of the X-ray emission comes from thermal re-processing (for example absorption and re-radiation by nearby matter), only a small fraction ( $<2\%$ ) of the total  $\gamma$ -ray energy could have been ‘thermalized’, unlike what one expects from an explosive event taking place close to the surface of a neutron star (the well-known ‘X-ray paucity’ constraint). We point out that, at least for this event, the spectra preclude a simple thermal origin for the X-ray emission. Although the ratio of 3–10 keV emission to  $>30$  keV emission was quite high ( $\sim 7$ – $20\%$ ) for this event, the fraction that could have come from a black-body component is constrained to be 2% or less. We

note the total X–ray emission from GRB 970228 was similarly high (Costa et al 1997).

It is difficult to compare the <few keV behavior of GRB 780506 with that of many *Ginga* bursts, as the angle of the burst to the detectors was unknown for many events, and uncertainty in response is greatest at these lowest energies. A few bursts were localized by other spacecraft. Of these, in GRB 900126 (localized by WATCH), a low energy turnover, consistent with absorption, is visible; while in GRB 910429 (localized by BATSE) there is at best a suggestion of flattening below a few keV. In BATSE data, sometimes the lowest channel of the spectroscopy detectors measured as low as a few keV. Out of  $\sim 100$  bursts, Preece et al. (1996) found  $\sim 10$ – $15\%$  showed low energy emission significantly in excess above the spectrum extrapolated from higher energies; and about an equal number with low energy roll–offs.

The strong low energy turnover seen at the onset of GRB 780506 serves as a reminder that soft X–ray photons might be removed from an observed burst spectrum by processes where the cross section is much higher for soft X–ray photons than for  $\gamma$ –rays, such as photo-electric absorption; Compton scattering in extended cold material; or magnetic field processes such as “cyclotron scattering”. Liang (1994) has proposed a cold absorption model where the absorbing material is Fe–rich. Although the GRB 780506 spectra are consistent with this simple picture of hard–to–soft evolution due to an optically thick absorbing layer being heated or blown away, there is no evidence of the predicted absorption edge at  $\sim 7$  keV or K-alpha emission feature at  $\sim 6.7$  keV. Brainerd (1994) has proposed a Compton attenuation model which both suppresses the low energy emission and predicts an X–ray afterglow. The  $\gamma$ –ray burst is assumed to be attenuated by scattering and absorption through dense molecular clouds. However the absorption edge would be red–shifted; and with this model, there is not a natural explanation for how the heaviest absorption should be on the rising edge of a burst. McBreen, Plunkett, and Metcalfe (1993) invoke a thick cocoon of material around a source of a relativistic beam of radiation; and show a slow–down of the beamed material producing an evolving beaming factor, to get the characteristic hard–to–soft spectral evolution. But the optical depth does not change in their scenario, so it is difficult to see how an evolving low–energy turnover would be produced. Liang et al. (1997) explicitly model this characteristic spectral evolution with an expanding, cooling plasma for which the Thomson depth decreases as the plasma thins. However the  $< 100$  keV portions of their spectra do not seem to match the flattening that was seen here.

The dramatic recent detections of several optical afterglows, one possibly associated with a galaxy (GRB 970228; van Paradijs et al. 1997) and one with absorption lines (GRB 970508; Metzger et al. 1997) apparently indicating a redshift of  $Z \sim 0.83$ , have focused attention on cosmological expanding fireball models (Mészáros and Rees 1997, henceforth MR97; Sari and Piran 1996; and references therein). These are modeled as relativistic shocks, with the burst being the signature of shocks developed internal to the ejecta wind (e.g., Pilla and Loeb 1998); and longer time–scale emission from external shocks produced as the ejecta plows into the local interstellar medium. This is a very appealing picture, but again we note that in detail, our  $< 50$  keV spectra do not match at least these preliminary predictions. In these models, for the

canonical GRB spectrum we described in the third paragraph of this section, the break energy at hundreds of keV is modeled as either due to inverse Compton (IC) or to the synchrotron peak (MR97; Katz et al 1997). Under very general assumptions, for a relativistic shock, the photon power-law index for the spectrum below the synchrotron peak should asymptotically approach  $0.7 - 1.5$ . Cohen et al. (1997), using the ( $> 20$  keV) spectra of 11 bright BATSE bursts, assume the few hundred keV break to be the synchrotron peak, and find moderate consistency. However, following their method of fitting the lowest energy channels by eye (but we used photon power-law spectra, while they used  $F_\nu$  spectra), we find, for the average spectrum of each peak (Figure 3), asymptotic slopes of  $\sim 0.5$  and  $1.9$  (equivalent to  $-1.5$  and  $-0.1$  in  $\nu F_\nu$  units). For the individual 10.24 s spectra (Figure 4) we find asymptotic slopes of  $\sim -0.7, 0.5, 0.3, 0.7, 2.3,$  and  $3.3$ ; which are widely outside these limits. One could argue that the initial low energy turnover is due to an evolving synchrotron peak (MR97), as it is emphasized by all authors that its position is unknown (Cohen et al 1997, Katz et al 1997). In this case the higher energy peak would be due to inverse Compton (which is also what Brainerd 1994 suggests). However we note that among the ensemble of historical measurements of X-rays from  $\gamma$ -ray bursts there are many with shapes outside the predicted low-energy limits (Laros and Nishimura 1986); and some, such as GRB 811016, have strong low energy suppression in the middle of the burst, precluding a simple evolving synchrotron interpretation (Katoh et al. 1984). There are now more complex kinds of cosmological theories: for example, Katz (1997) emphasizes the difficulties of realistically producing  $\gamma$ -rays with complex time-histories in these scenarios, and instead suggests pulsar-like emission.

From just these *HEAO 1* A-2 data, it is hard to distinguish among:  $N_H$  absorption plus Compton attenuation, followed by black body emission or soft X-rays forward-scattered by dust (Brainerd 1994);  $N_H$  absorption plus Compton down-scattered flux (Yaqoob 1997); a moving synchrotron peak from a relativistic expanding fireball model; as well as the effect of a possible red-shift on the absorption edge. Future experiments with good energy resolution below a few keV may be able to distinguish among these (Forrest et al. 1995).

## 2.6. Afterglow Light Curve

In Figure 5 we display the light-curve of just the X-ray afterglow, in 122.88 s bins, along with the A-2 HED3 Layer 1 2-20 keV rates for the same times. One sees a peak at about 7 minutes ( $\pm 1$  minute) after burst onset. When exponential models are used to fit the rise (first two bins plus the peak) and decay (peak plus the last thirteen points in this orbit), one finds time-scales of  $190 \pm 80$  s with  $\chi^2 = 0.3$  for 1 d.o.f., and  $2090 \pm 1430$  s with  $\chi^2 = 21$ . for 12 d.o.f., respectively. We note that the ‘decay’ portion was not well-fit by this simple model. We suggest that afterglow variability on time-scales on the order of  $\sim \frac{1}{2}$  hr is potentially interesting, and should be investigated in the future. We also tried plotting the burst and afterglow on a log-log scale to see if there was a discernible power-law decay envelope (Costa et al. 1997), but this only seemed to accentuate the variability of this event. In particular, Costa et al. (1997) extrapolate

their GRB 970228 afterglow measurement to be part of a power-law decay of the burst itself. In contrast, here, there seemed to be a clear break between the X-rays from the burst and the rise to the afterglow: a different phenomenon than the decay of an X-ray tail lasting minutes observed by Vela (Terrell et al. 1982) and *Ginga* (Yoshida et al. 1989; Murakami et al. 1992).

At shorter timescales, an FFT of this time interval, using 5.12 s time bins, yielded a 90% upper limit of  $< 2\%$  on any pulsed component less than 15 minutes.

Qualitatively, one might argue that this afterglow could be the signal of the relativistic plasma that produced the burst encountering the local interstellar medium (MR97). Alternatively, Katz et al. (1997) considers the source sputters (in gamma-rays as well as lower energies) at a much lower level for on the order of a day before and after the bright “burst” portion. Quantitatively, however, these models still have many unknowns. We note the afterglow spectrum is too soft to be an extrapolation of flux below the synchrotron peak, for example (Cohen et al. 1997 and references therein). Future high signal-to-noise measurements of spectra and light-curves during this interesting time, from directly after a burst until several hours after, would be useful in shaping these models (Smith et al. 1998; Takeshima et al. 1998).

We asked the question, what were our limits on longer timescale (several hour) emission from the burst source, excluding the afterglow? When times of high particle background were excluded (MacIlwain’s  $L$ -parameter restricted to  $\leq 1.4$ ), we obtain a  $2\sigma$  upper limit on persistent emission from the burster of  $< 3$  millicrabs ( $0.005 \text{ cts-cm}^{-2}\text{-s}^{-1}$ ) using scanning data for several days after the burst and afterglow. We found no evidence of significant emission before the burst, but point out that the Earth’s disk would have occulted any emission from the source between  $\sim \frac{1}{2}$  hr to 10 s before the beginning of GRB 780506.

At higher energies ( $\geq 100$  keV), Klebesadel et al. (1984), Klebesadel (1992), and R. Klebesadel (1985, private communication), describe an event observed by PVO, GRB 840304, composed of 2 intense,  $\sim 30$  s FWHM peaks, 100 s apart, which were followed by  $\sim 1500$  s of emission about two orders of magnitude fainter than the peak intensities. This extended emission had roughly an  $E^{-1.3}$  spectrum, much harder than the emission here. Klebesadel (1989) points out that the  $\sim 1500$  s duration is only a  $\sim 3\sigma$  deviation from the long duration tail of the distribution of event durations observed by PVO. At even higher energies, Hurley et al. (1994) describe extended GeV emission following GRB 940217, and remark on GeV emission detected  $\sim$ minutes after four other events. Since the spectra of these reports of extended emission are not consistent, it is not clear whether they are related phenomena.

### 3. Conclusion

In the past, longer time-scale X-ray emission from  $\gamma$ -ray bursts has been seen as an indicator of a separate thermal component (Laros and Nishimura 1986; Chernenko and Mitrofanov 1994). We argue above that the increase in X-ray time-scales follows the same pattern observed at

$\gamma$ -ray energies, and that the energy in 2–60 keV X-rays is released through the same non-thermal processes that generate the  $\gamma$ -ray emission. This pattern of spectral variability is visible in the X-ray spectra as well as the light-curves. We have argued that when viewed in detail, the 2-60 keV X-ray emission shows no unambiguous evidence for a thermal interpretation. We set a limit of  $<2\%$  on the black-body component of the emission. Unlike some *Ginga*  $\gamma$ -ray bursts, there was no evidence for line-features. Instead, the general trend seems to be a non-thermal power-law in the X-rays below the characteristic break energy or maximum in  $\nu F_\nu$  (typically  $\sim 200$  keV but with a wide range; here,  $\sim 45$  keV). Below a few to  $\sim 10$  keV this evolves to either a turnover consistent with high intrinsic absorption or excess soft emission (Strohmayer et al. 1998; Preece et al. 1996). There was no evidence to suggest the second peak was part of an afterglow that was distinct from the burst itself, unlike GRB 970228 (Costa et al. 1997; 1998). We note that, like many bursts measured previously in X-rays, the spectral shape varies widely outside low-frequency limits predicted by current relativistic shock models.

Two characteristics of GRB 780506 may be unusual. One is the softer than average  $>45$  keV spectrum, placing it in the “NHE” subclass (see Pizzichini et al. 1995; Kouveliotou et al. 1996; Belli 1997; and Pendleton et al. 1997). The more dramatic is its faint,  $\sim 1$  keV afterglow. Extended emission has now been detected from at least seven of nine bright  $\gamma$ -ray bursts that have had extensive multi-spacecraft follow-up (Paczynski and Kouveliotou 1997 and references therein; Heise et al. 1997; Piro et al. 1998a,b; Halpern et al. 1997). However these detected apparently fading emission, on timescales of hours or days, not the initial resurgence of soft X-rays reported here. Also, though extended emission had been detected at higher energies ( $>100$  keV, Klebesadel et al. 1984; Klebesadel 1992;  $>100$  MeV, Hurley et al. 1994), it is not clear these are the same phenomena.

For the afterglow, it is not clear whether it is the rare, long-duration tail of the overall  $\gamma$ -ray burst duration distribution (Klebesadel 1992; Kouveliotou et al. 1994); or whether the  $\sim 1$  keV emission, few minute rise time, irregular flux and potential  $\frac{1}{2}$  hr decay are characteristic of most  $\gamma$ -ray bursts. This is a new regime. First, earlier instruments with wide fields of view also tended to have high backgrounds due to source confusion (see Laros and Nishimura 1986 and references therein). Second, burst monitors such as those on *BeppoSAX* have historically stored data for only a limited time after a burst (e.g. Boella et al. 1997). Recently, the *RXTE* ASM and the WFC on board *BeppoSAX* have begun to accumulate data on  $\gamma$ -ray bursts observed at least minutes after burst onset, and may be able to set constraints in the near future (Smith et al. 1998; Takeshima et al. 1998; Piro et al. 1998a,b). If this resurgent X-ray afterglow is a feature common to many  $\gamma$ -ray bursts, and if it is accompanied by optical emission, then there may be a  $\sim 60$  minute window (rather than a one minute window) during which it is possible to observe brighter optical emission associated with a  $\gamma$ -ray burst.

For the burst itself, it remains for future experiments with good signal-to-noise below a few keV such as *HETE* (Ricker et al. 1992) and *CATSAT* (Forrest et al. 1995); or more extended observations of GRBs from current satellites such as *RXTE* (Takeshima et al. 1998; Smith et al.

1998) and the Italian–Dutch satellite *BeppoSAX* (Boella et al. 1997) to determine to what extent the generally non–thermal spectrum; the hard–to–soft variability; and the low energy turnover evolving to slight excess  $\sim 1$  keV emission; are characteristics of X–rays from all  $\gamma$ –ray bursts.

The GRO/COMPTEL group at UNH’s Institute for the Study of Earth, Oceans and Space, under J. Ryan, provided support throughout. This work was supported through NASA grant NAG 5-1753, which included funds for the purchase of a workstation. This research has made use of data obtained through the High Energy Astrophysics Science Archive Research Center Online Service, provided by NASA–Goddard Space Flight Center.

## A. Two Bayesian Methods for Finding the Position of a Variable Source

### A.1. Overview

We have derived and applied two Bayesian likelihood ratios for the problem of finding the position of a time–varying source from comparisons of detector rates. This Bayesian formalism allowed one to integrate over the unknown light–curve shape, parametrized by  $\{s_k\}$ , freeing one to handle datasets with many more time bins, in which the true source intensity and positions of the detector axes were allowed to vary. Loredo (1990, 1992) and Gregory & Loredo (1992; henceforth GL92) suggest that Bayesian methods can extract the maximum amount of information when carefully applied to data analysis problems. The first Bayesian likelihood ratio, for a high signal–to–noise Gaussian approximation, was simpler and more efficient. In the Poisson case, necessary for faint sources, although the likelihood ratio was more complex and the calculation more computer–intensive, the constraints on position were tighter. It should be straightforward to apply this same process, to data from other detectors, where Bayesian methods could be expected to give an improved result.

Sampling statistics deals with data–space, with  $p(D|\Omega, \mathcal{H}, I)$ , the *direct probability* of the data  $D$  given an hypothesis or model  $\mathcal{H}$  with parameters  $\Omega$  and prior information  $I$ . In Bayesian inference one works in parameter–space, with the probability of the parameters  $\Omega$  given the model  $\mathcal{H}$  plus prior information  $I$ ,  $p(\Omega | D, \mathcal{H}, I)$ . Formally, one calculates one from the other via Bayes’s theorem, (a consequence of the product rule of probability):

$$p(\Omega | D, \mathcal{H}, I) = p(\Omega | \mathcal{H}, I)p(D | \Omega, \mathcal{H}, I)/p(D | \mathcal{H}, I) \tag{A1}$$

The concept is that one *updates* the *prior probability*  $p(\Omega | \mathcal{H}, I)$  with the *direct probability* of the data  $p(D | \Omega, \mathcal{H}, I)$ , normalized with  $p(D | \mathcal{H}, I)$ , to get the *posterior probability*  $p(\Omega | D, \mathcal{H}, I)$ .

One benefit of working in parameter space is the ability to integrate over uninteresting parameters. For the application presented here, one integrates analytically over unknown light–curve parameters, and numerically over the measured background rates, to obtain a

likelihood ratio parametrized only by the unknown source position  $(\phi, \theta)$ . The final output is a map of this Bayesian likelihood ratio as a function of  $(\phi, \theta)$ . Position constraints are found by drawing contours of constant log probability around regions of highest probability, or credible regions (GL92; Loredo 1990; Loredo 1992).

The two algorithms we derived, high and low signal-to-noise likelihood ratios, were tested on *HEAO 1* A–2 proportional counter data from sources with known positions. However, the algorithms should be applicable to any source observed by multiple detectors with overlapping, well-understood spatial responses; similar spectral responses; and predictable backgrounds. These algorithms were then applied to both GRB 780506 and the  $\sim 50$  minute 2–20 keV emission observed following it. Originally, Connors (1988) had tried a maximum likelihood method. The improved position constraints from the Poisson Bayesian likelihood ratio strengthen the hypothesis that this emission is associated with the burster itself, rather than coming from a serendipitous source (Connors and McConnell 1996).

## A.2. Data

The position-finding algorithms derived here were first tested on a variety of *HEAO 1* A–2 data: scanning and pointed data; on bright and faint sources. These are listed in Table 2. During the Crab observation, the detector look-direction rotated at about  $1^\circ$  every 5 seconds. During the other observations the detector axes rocked by about  $1^\circ$  on timescales of minutes. Since the derivation assumes the background to be constant, we chose data that was the least sensitive to particle contamination: MED Layer 1 rates, restricted to times of high rigidity (MacIlwain’s  $L$ -parameter restricted to  $L < 1.2$ ).

These algorithms were then applied to sources with unknown positions: GRB 780506 and the following soft X-ray emission.

## A.3. Previous Method: Maximum Likelihood

The earlier position-finding algorithm (of Connors 1988) was a maximum likelihood method, with the position  $(\phi, \theta)$  of the source; the rate  $\{s_k\}$  in each time bin; and the (constant) background  $b_j$  in each field of view, as parameters. Let  $\epsilon_{jk}(\phi, \theta)$  represent the detector effective area of the  $j^{\text{th}}$  detector field of view as a function of source position  $(\phi, \theta)$  at time  $t_k$ . Then the total expected rate  $\mu_j$  in the  $j^{\text{th}}$  detector field of view at time  $t_k$  can be modeled as:

$$\mu_{jk}(\phi, \theta) = b_j + s_k \epsilon_{jk}(\phi, \theta). \tag{A2}$$

In Connors (1988), the background parameters  $b_1$  and  $b_2$  were determined from previous measurements; and the detector effective areas  $\epsilon_{jk}$  were determined from calibrations with known



sources; so only the source position  $\phi, \theta$  and its intensity as a function of time, as parametrized by the  $s_k$ , were unknown. Following the maximum likelihood approach of Cash (1978), the light–curve parameters  $\{s_k\}$  are allowed to freely float until one finds the maximum probability for that  $\phi, \theta$  position. However the maximum likelihood method required independent fit–parameters for the source intensity in each time bin. For transients with durations of order roughly minutes, this meant at worst dozens of light–curve parameters. For sources observed for an hour, one would need closer to  $10^3$  independent parameters. This was not practical. One could bin the data into longer time bins; however since even during pointed observations, the detector point–direction varied, positional information could be lost.

This was the case for the  $\sim 50$  minute emission that followed GRB 780506.

#### A.4. First Bayesian likelihood ratio: high signal–to–noise

In the previous section, both the background parameters  $b_1, b_2$  and the unknown light–curve parameters  $s_k$  could have been considered “nuisance” parameters that made finding constraints on the source position computationally difficult. In this section, one uses a Bayesian approach to integrate over them, with the simplifying assumption that a Gauss–Normal distribution is a reasonable approximation of the Poisson distribution. This works well when the signal is at least several  $\sigma$  above the background in each time bin.

First, one specifies prior probabilities for each of the parameters,  $p(s_k | I), p(b_1 | I)$ , and  $p(b_2 | I)$ . When there is no prior measurement, for parameters describing a rate, GL92 uses an invariance argument to suggest a uniform prior over a range  $s_0$  to  $s_1$ , where  $s_0$  might be zero, and  $s_1$  the maximum rate the detectors can measure:  $p(s_k | \mathcal{H}, I) = \frac{1}{s_1}$ . For the backgrounds  $b_1$  and  $b_2$ , there are prior measurements:  $B_1$  and  $B_2$  counts in times  $T_1$  and  $T_2$ , in detector fields–of–view 1 and 2, respectively. Therefore the appropriate expressions for the prior probabilities on  $b_1$  and  $b_2$  are (Loredo 1990)

$$p(b_1 | B_1, T_1, I) = e^{-b_1 T_1} \frac{(b_1 T_1)^{B_1}}{B_1!} \quad \text{and} \quad p(b_2 | B_2, T_2, I) = e^{-b_2 T_2} \frac{(b_2 T_2)^{B_2}}{B_2!}. \quad (\text{A3})$$

One combines them with the direct probability, using Bayes’s Theorem, to obtain the posterior probability. For this section, the direct probability is assumed to be Gaussian.

First, one deals with the  $s_k$ . One integrates (marginalizes) analytically over each  $s_k$ , then takes the product over all  $k$  data bins, with  $y_{jk}$  counts in each data bin, the mean given by equation A2, and its associated  $\sigma_{jk}$  given by  $\sigma_{jk} = \sqrt{y_{jk}}$ . In the limit where the Gaussian dsitribution in  $s_k$  is sharply peaked compared to the width of the integration interval  $[0, s_1]$ , one obtains a simplified expression for the (negative) log of the posterior probability  $\lambda(b_1, b_2, D1, D2 | \phi, \theta, \mathcal{H}) \propto -\log[p(b_1, b_2, D1, D2 | \phi, \theta, I)]$ :

$$\lambda(b_1, b_2, D1, D2 | \phi, \theta) =$$

$$-\left(B_1 - b_1 T_1 + B_1 \log\left(\frac{b_1 T_1}{B_1}\right)\right) - \left(B_2 - b_2 T_2 + B_2 \log\left(\frac{b_2 T_2}{B_2}\right)\right) + \frac{1}{2} \sum_{k=1}^N \frac{(\Delta_{1k} - \Delta_{2k})^2}{\sigma_{Tk}^2}, \quad (\text{A4})$$

where

$$\sigma_{Tk} \equiv \sqrt{(\sigma_{1k}\epsilon_{2k})^2 + (\sigma_{2k}\epsilon_{1k})^2}, \quad (\text{A5})$$

and

$$\Delta_{1k} \equiv (y_{1k} - b_1) \epsilon_{2k}; \quad \text{and} \quad \Delta_{2k} \equiv (y_{2k} - b_2) \epsilon_{1k}. \quad (\text{A6})$$

If one or more of the detector effective areas  $\epsilon_{jk}$  were zero, the appropriate term(s) in the sum would be replaced by:

$$\left(\frac{y_{2k} - b_2}{\sigma_{2k}}\right)^2 \text{ for } \epsilon_{1k} = 0; \quad \text{or} \quad \left(\frac{y_{1k} - b_1}{\sigma_{1k}}\right)^2 \text{ for } \epsilon_{2k} = 0; \quad (\text{A7})$$

or by

$$\log(s_1) + \left(\frac{y_{1k} - b_1}{\sigma_{1k}}\right)^2 + \left(\frac{y_{2k} - b_2}{\sigma_{2k}}\right)^2 \quad (\text{A8})$$

for  $\epsilon_{1k} = 0$  and  $\epsilon_{2k} = 0$ .

Second, one numerically integrates the negative exponential of this form over  $b_1$  and  $b_2$  to obtain  $\mathcal{L}(D1, D2 \mid \phi, \theta, \mathcal{H}) \propto \log[p(D1, D2 \mid \phi, \theta, I)]$ , the log-likelihood of the data given source positions  $(\phi, \theta)$ . For each position in a grid of  $(\phi, \theta)$ , one first found the minimum of  $\lambda$ ,  $\lambda_0$ ; and then numerically integrated  $\exp\{-\lambda + \lambda_0\}$  over the background parameters  $b_1$  and  $b_2$ . The minimization used a modified Levenberg–Marquardt algorithm, which returns both a best-fit for each parameter and an estimate of its  $\sigma$ , using the curvature to find a Gaussian approximation. (Bevington 1969; Press *et. al.* 1986 and references therein). The numerical integration used Gaussian quadrature, with Gaussian weights, assuming the  $\sigma$  found in the previous step, and using Hermite polynomials (Scheid 1968; Abramowitz & Stegun 1972; Press *et. al.* 1986), typically with eight roots.

For the data tried here, the whole procedure was relatively fast, requiring about two hours of Decstation 5000/125, (or one hour of 40 MHz Sparc 10) CPU time for 852 time bins and  $10^3$  grid-points. The computer time scaled linearly with the number of time bins in the data-set and grid-points requested.

Third, one maps out contours of constant  $p(\phi, \theta \mid D1, D2, I)$ , assuming a uniform prior on  $\phi, \theta$ , to obtain constraints on the parameters. Position constraints are delineated by contours of constant log probability drawn to contain regions of highest posterior probability, or Credible Regions (Loredo 1992 and references therein). We used Credible Regions containing 95.45% and 97.23% of the posterior probability to delineate the source positions.

### A.5. Application to Data: Known and Unkown Sources

This high signal-to-noise algorithm was tested on data from several known point sources. The first panel of Figure 6 shows the results, plotted in two grayscale contours, for 5 scans (182 time bins) across the Crab nebula plus pulsar (on D.O.Y. 1977 260). The second panel shows the results from 2.5 hr (632 time bins) from the pointed observation of the highly variable neutron-star binary GX 301-02 (on D.O.Y. 1978 25). The last two panels show the results on a pointed observation of the cluster Abell 401 (D.O.Y. 1978 39). The left panel displays the results on the entire point (832 time bins), while the right shows the results for a single orbit (352 time bins). The latter is analogous to the data from the unknown source following GRB 780506, for which data from a single orbit was used. For each plot, the darker contour encloses a 99.45% ( $2\sigma$ ) credible region, and the lighter a 99.73% ( $3\sigma$ ) credible region. The true source positions are marked with an asterisk. It is clear that the high signal-to-noise algorithm works for the bright test cases, but is a little off (although still within  $3\sigma$ ) for the faintest source, Abell 401. This will be addressed when using the full Poisson method, for lower signal-to-noise data.

Next, this algorithm was used to constrain the position of GRB 780506 and the position of the unknown transient that occurred just afterwards. These are *HEAO 1 A-2* 5.12 s rates from the first layer of the offset High Energy Detector, HED1, with data constrained to MacIlwain’s  $L$ -parameter  $L < 1.4$ , obtained during the first orbit following GRB 780506 (Figures 1 and 3). For Figure 7, the GRB 780506 95.45 and 99.73% credible regions were plotted in gray contours, while those for the extended emission were overplotted as line contours. The error box for GRB 780506 changed little from that in Connors (1988). However, the position constraints for the fainter transient changed appreciably. The Bayesian algorithm allowed for variations in intensity in each time bin, while because of the large number of intensity parameters that would have been required, the likelihood method could not. This suggests the position contours displayed in Figure 7 are the more physically realistic constraints. However, recall that in two places in the derivation, one assumed the signal was at least several  $\sigma$  above the background in each time bin. This is not strictly true for the faint  $\sim 50$  minute emission. In the next section, we sketch out the analogous derivation, but without that simplifying assumption.

### A.6. Second Bayesian likelihood ratio: low signal to noise

Here, one follows the same steps as in the previous section: writing down the joint sampling probability; using the same priors, marginalizing analytically over the  $s_k$ ; then numerically over the background rates; but for the full Poisson expression necessary when measuring faint sources. In order to do this, one defines a numerically convenient log-likelihood analogous to equation (A4). The output will be the log of a global likelihood ratio.

These expressions will be more difficult to compute than for the Gaussian approximation above, but provide better constraints for the low signal-to-noise cases.

Instead of a Gauss–Normal approximation for the sampling (direct) probability, one starts with the Poisson expression for the joint probability for a single time bin. One again uses a uniform prior on the  $s_k$ , marginalizes over each  $s_k$ , and takes the product over all  $k$  time bins. The log of the resulting expression likelihood is not as simple as that for the Gaussian approximation, but straightforward to calculate:

$$\lambda(D1, D2 | b_1, b_2, \phi, \theta, I) = \left( b_1 T_1 - B_1 + B_1 \log\left[\frac{B_1}{b_1 T_1}\right] \right) + \left( b_2 T_2 - B_2 + B_2 \log\left[\frac{B_2}{b_2 T_2}\right] \right) + N(b_1 + b_2) - \sum_{k=1}^N \log \left( \sum_{l_{1k}=0}^{y_{1k}} \sum_{l_{2k}=0}^{y_{2k}} \binom{y_{1k}}{l_{1k}} \binom{y_{2k}}{l_{2k}} b_1^{y_{1k}-l_{1k}} b_2^{y_{2k}-l_{2k}} \frac{\epsilon_{1k}^{l_{1k}} \epsilon_{2k}^{l_{2k}}}{(\epsilon_{1k} + \epsilon_{2k})^{l_{1k}+l_{2k}+1}} (l_{1k} + l_{2k})! \right), \quad (\text{A9})$$

for  $\epsilon_{jk}$  non–zero; with the appropriate term in the sum over  $k$  replaced by

$$y_{2k} \log(b_2) + \log \left( \sum_{l_{1k}=0}^{y_{1k}} \binom{y_{1k}}{l_{1k}} b_1^{y_{1k}-l_{1k}} \frac{l_{1k}!}{\epsilon_{1k}} \right), \quad (\text{A10})$$

if  $\epsilon_{2k} = 0$  (or its equivalent if  $\epsilon_{1k} = 0$ ); or

$$y_{1k} \log(b_1) + y_{2k} \log(b_2), \quad (\text{A11})$$

if both  $\epsilon_{1k} = 0$  and  $\epsilon_{2k} = 0$ .

Again, for each  $\phi, \theta$  bin,  $\min(\lambda(D1, D2 | b_1, b_2, \phi, \theta, I)) = \lambda_0$  was found, and the exponential of  $(-\lambda(D1, D2 | b_1, b_2, \phi, \theta, I) + \lambda_0)$  was numerically integrated over  $b_1$  and  $b_2$ .

Unlike for the Gaussian approximation, these calculations were very slow, requiring about  $\sim 70$  times as much CPU time. The computer time scaled linearly not only with the number of time bins in the data–set and grid–points requested, but with the average count–rate as well. In practice, then, one prefers to use this algorithm for short datasets with low count–rates. However, for these low signal–to–noise observations, the restriction of  $\{s_k\} \geq 0$  that is implicit in the Poisson formulation led to tighter and more accurate constraints on position.

### A.7. Application to Data: Known and Unknown Sources

As a test of this algorithm, we used HEAO1 A–2 MED data from a pointed observation of the faintest test source, Abell 401. Shown in Figure 8 are position contours for both one orbit (about one hour; 352 time bins) of data, and for the whole point (about three hours; 852 time bins).

Finally, the full Bayes Poisson algorithm was used on the unidentified transient following GRB 780506. From comparing Figure 9 to Figure 7, one sees that the position contours for the  $\sim 50$  minute emission shrank. That should not be surprising. The longer time–scale emission was not many  $\sigma$  above background, and by using the Poisson distribution, one smoothly incorporates

an implicit constraint that all the light-curve parameters  $\{s_k\}$  are non-negative. Notice that using the Poisson expression was important even when the total average count-rate was above 30, when the source signal was faint compared to background (Loredo 1990). (The contours visible in the upper left, although formally allowed by the HED 1 data alone, were ruled out after the fit by the lack of signal in the HED 2 data.) Since this error-box has about an order of magnitude smaller area than the previous error box, it strengthened the supposition that this  $\sim 50$  minute X-ray glow came from the same source as the  $\gamma$ -ray burst (Connors and McConnell 1996).

Table 1. Shape of the spectra for 7 time intervals

No.	$\chi^2$	Black body component			Power law component		$N_H$ $10^{23}$ $\text{cm}^{-2}$
	for 31 DOF	$A_1$ $\times 10^3$	Radius km @ 1kpc	kT keV	$A_2$	$\alpha$	
1	26.9	$.17 \pm .01$	$.04 \pm .004$	$6.4 \pm 2.0$	$.47 \pm .004$	$1.16 \pm .01$	$.3 \pm .05$
2	26.0	$1.6 \pm .1$	$.12 \pm .01$	$2.6 \pm .05$	$.085 \pm .005$	$1.56 \pm .03$	$0. \pm .01$
3	25.6	$6.9 \pm .4$	$.26 \pm .03$	$1.85 \pm .03$	$.19 \pm .006$	$1.44 \pm .01$	$0. \pm .006$
4	27.0	$3.8 \pm .4$	$.19 \pm .04$	$1.76 \pm .05$	$.40 \pm .01$	$1.87 \pm .02$	$0. \pm .004$
5	11.4	$37. \pm 6.$	$.60 \pm 0.2$	$0.85 \pm .03$	$.24 \pm .02$	$2.34 \pm .04$	$0. \pm .008$
6	13.3	$120. \pm 100.$	$1.1 \pm 0.9$	$0.45 \pm .09$	$.28 \pm .03$	$2.91 \pm .07$	$0. \pm .1$
7	8.2	$1 \cdot 10^3 \pm 2 \cdot 10^2$	$3.1 \pm 1.2$	$0.42 \pm .01$	$.093 \pm .02$	$2.21 \pm .1$	$0. \pm .1$

Table 2: Observations Used for Position-Finding Algorithms

Source Name	D.O.Y. 1977	No. of 5.12 s Bins	Peak Source Rates		Average Background rates	
			Large FOV $\frac{\text{cts}}{5.12 \text{ s}}$	Small FOV $\frac{\text{cts}}{5.12 \text{ s}}$	Large FOV $\frac{\text{cts}}{5.12 \text{ s}}$	Small FOV $\frac{\text{cts}}{5.12 \text{ s}}$
Crab <sup>s,a</sup>	260	182	2160	1743	$23.3 \pm 1.5$	$13.4 \pm 1.2$
GX301-02 <sup>p,a</sup>	390	632	114	80	$23.6 \pm 1.5$	$13.6 \pm 1.2$
Abell 401 <sup>p,b</sup>	404	832	49	35	$23.9 \pm 1.5$	$13.6 \pm 1.2$
Abell 401 <sup>p,b</sup>	404	352	49	35	$23.9 \pm 1.5$	$13.6 \pm 1.2$
GRB 780506 <sup>p,c</sup>	491	24	1386	1012	$56.2 \pm 0.4$	$30.1 \pm 0.3$
Afterglow <sup>p,c</sup>	491	464	88	51	$56.2 \pm 0.4$	$30.1 \pm 0.3$

<sup>s</sup>Scanning data

<sup>p</sup>Pointed data

<sup>a</sup>Source position from Bradt and McClintock (1984).

<sup>b</sup>Source position from SIMBAD.

<sup>c</sup>Source position from this work.

## REFERENCES

- Abramowitz, M. & Stegun, I., 1972, *Handbook of Mathematical Functions*, (New York: Dover Publications, Inc.)
- Band, D., et al. 1992, in *Gamma-Ray Bursts*, AIP Conf. Proc. 265, eds. W. S. Paciesas & G. B. Fishman, (New York: AIP Press), p 169
- Band, D., et al. 1993, ApJ, 413, 281
- Boella, G., et al., 1997, A&AS, 122, 299
- Belli, B. M., 1997, ApJ, 479, L31
- Bevington, P. R., 1969, *Data Reduction and Error Analysis for the Physical Sciences*. (New York: McGraw-Hill)
- Bradt, H. V. D., & McClintock, J. E. 1984, ARA& A, 21, 13
- Brainerd, J. J., 1994, ApJ, 428, 21
- Cash, W., 1978, ApJ, 228, 939
- Chernenko, A. M. & Mitrofanov, I. G., 1994, *Gamma-Ray Bursts*, AIP Conference Proc. No 307, ed G. J. Fishman, J. J. Brainerd, & K. Hurley (New York: AIP) 293
- Chernenko, A. M., et al., 1998, in *Proceedings of the 4th Huntsville Symposium on Gamma-ray Bursts* AIP Conference Proc. 428, Meegan, C. A., Preece, R. D. & Koshut, T. M. (New York: AIP), 30
- Chipman, E., 1994, *Gamma-Ray Bursts*, AIP Conference Proc. No 307, ed G. J. Fishman, J. J. Brainerd, & K. Hurley (New York: AIP) 202
- Cline, T. L., et al. 1979, ApJ, 232, L1
- Cohen et al. 1997, ApJ, 488, 330
- Connors, A. 1988, Ph.D. thesis, University of Maryland
- Connors, A., Serlemitsos, P. J., & Swank, J. H., 1986, ApJ, 303, 769
- Connors, A. & McConnell, M. 1995, in Proc. 24th Int. Cosmic-Ray Conf., Rome, Italy, 2, 57
- Connors, A. & McConnell, M. M., 1996, in *Proc. of the 3rd Huntsville Symposium on Gamma-Ray Bursts AIP Conf. Proc. 384*, ed. C. Kouveliotou, M. F. Briggs, & G. J. Fishman, (New York: AIP) 607
- Costa, E., et al., 1997, Nature, 387, 783
- Costa, E., et al., 1998, in *Proceedings of the 4th Huntsville Symposium on Gamma-ray Bursts* AIP Conference Proc. 428, Meegan, C. A., Preece, R. D. & Koshut, T. M. (New York: AIP), 409
- Dingus, B., et al., 1994, *Gamma-Ray Bursts*, AIP Conference Proc. No 307, ed G. J. Fishman, J. J. Brainerd, & K. Hurley (New York: AIP) 22

- Epstein, R. I., 1986, in *Radiation Hydrodynamics in Stars and Compact Objects*, Proceeding of IAU Colloquium 89, (Spring Verlag: New York) eds. K.-H. Winkler & D. Mihalas) 305
- Fenimore, E. E. et al., 1988, ApJ, 335, L71
- Fenimore, E. E., in 't Zand, J.J.M., Norris, J.P., Bonell, J. T., & Nemiroff, R. J. 1995, ApJ, 488, L101
- Fishman, G. et al., 1994, ApJS, 92, 229
- Ford, L., Band, D., Matteson, J., Teegarden, B. & Paciesas, W. 1994, *Gamma-Ray Bursts*, AIP Conference Proc. No 307, ed G. J. Fishman, J. J. Brainerd, & K. Hurley (New York: AIP) 298
- Forrest, D., et al., 1995, Ap&SS, 231, 459
- Gilman, D., Metzger, A. E., Parker, L. H., Evans, L. G., & Trombka, J. I., 1980, ApJ, 236, 951
- Graziani, C., Fenimore, E. E., Murakami, T., Yoshida, A., Lamb, D. Q., Wang, J. C. L., & Loredo, T. J., 1992, in *Gamma-Ray Bursts: Observations, Analyses and Theories*, eds. C. Ho, R. I. Epstein, & E. E. Fenimore (Cambridge: Cambridge University Press), 407
- Gregory, P. C., & Loredo, T. J. 1992, ApJ 398, 146 (GL92)
- Halpern, J., et al., 1997, IAU Circ. 6788.
- Heise, J., et al., 1998, in *Proceedings of the 4th Huntsville Symposium on Gamma-ray Bursts* AIP Conference Proc. 428, Meegan, C. A., Preece, R. D. & Kosshut, T. M. (New York: AIP), 397
- Heise, J., et al., 1997, IAU Circ. 6787
- Hueter, G., 1987, Ph.D. thesis, University of California at San Diego
- Hurley, K., *et. al.*, 1994 Nature, 372, 652
- Imamura, J. N. and Epstein, R. I. , 1987 ApJ, 313, 711
- Kargatis, V.E., Liang, E.P., Hurley, K. C., Barat, C., Evans, E., & Niel, M., 1994, ApJ, 422, 260
- Katoh, M., Murakami, T., Nishimura, J., Yamagami, T., Tanaka, Y., & Tsunemi, H., 1984, in *High Energy Transients in Astrophysics*, AIP Conference Proc. No 115, ed S. E. Woosley (New York: AIP), 390.
- Katz, J., 1997, ApJ, 490, 633.
- Katz, J. I., Piran, T., & Sari, R., 1997, submitted to Phys Rev. B.
- Kerr, F. J., Bowers, P. F., Jackson, P. D., & Kerr, M. 1986, A&ASS, 66, 373
- Kippen, R. M., et al., 1997, Adv. Space Res., in press
- Klebesadel, R., Laros, J., & Fenimore, E., 1984, BAAS, 16, 1016
- Klebesadel, R. 1992, in *Gamma-Ray Bursts: Observations, Analyses and Theories* ed. C. Ho, R. I. Epstein & E. E. Fenimore (Cambridge: Cambridge University Press) 161



- Kouveliotou, C., Meegan, C. A., Fishman, G. J., Bhat, P. N., Briggs, M. S., Koshut, T. M., Paciesas, W. S., & Pendleton, G. N., 1994, in *Gamma-Ray Bursts*, AIP Conference Proc. No 307, ed G. J. Fishman, J. J. Brainerd, & K. Hurley (New York: AIP) 167
- Kouveliotou, C., et al. 1996, in *Proc. of the 3rd Huntsville Symposium on Gamma-Ray Bursts AIP Conf. Proc. 384*, ed. C. Kouveliotou, M. F. Briggs, & G. J. Fishman, (New York: AIP) 42
- Lang, K., 1980, *Astrophysical Formulae* (New York: Springer-Verlag)
- Laros et al., 1984, in *High Energy Transients in Astrophysics* ed. S. E. Woosley (New York: AIP) 378
- Laros et al., 1984, *ApJ*, 286, 681
- Laros, J. & Nishimura, J., 1986, in *Gamma-Ray Bursts*, AIP Conference Proceedings No 141, eds. E. P. Liang & V. Petrosian, (New York: AIP) 79
- Liang, E. P., 1994, in *Gamma-Ray Bursts*, AIP Conference Proceedings No 307, eds. G. J. Fishman, J. J. Brainerd, & K. Hurley, (New York: AIP) 351
- Liang, E. P., Kusunose, M., Smith, I. A., and Crider, A., 1997, *ApJ*479, L35
- Linsky, J. L., 1990, in *Imaging X-ray Astronomy*, ed. M. Elvis, (New York: Cambridge University Press) 39
- Loredo, T. J., 1990, in “Maximum Entropy and Bayesian Methods”, ed P. F. Fougere, (Dordrecht: Kluwer Academic Publishers), 81
- Loredo, T. J., 1992, in *Statistical Challenges in Modern Astronomy*, ed. G. J. Babu & E. D Fiegelson (New York: Springer-Verlag)
- Lucke, P. B. 1978, *A&A*, 64, 367
- Matteson, J. 1978, AIAA 16th Aerospace Sciences Meeting, paper 78-35
- Matz, S. M. et al. 1985, *ApJ*, 288, L37
- McBreen, B., Plunkett, S., & Metcalfe, L., 1993, *A&A, Suppl.*, 97, 81
- Mészáros, P. & Rees, M. J., 1997, *ApJ*, 476, 232
- Metzger, M. R., et al., 1997, *Nature*, 387, 878
- Motch, C., Belloni, T., Buckley, D., Gottwald, M., Hasinger, G., Pakull, M.W., Pietsch, W., Reinsch, K., Remillard, R.A., Schmitt, J.H.M.M., Trümper, J., & Zimmerman, M.W., 1991a, *A&A*, 246, L24
- Motch, C., Stella, L., Lanot-Pachero, E., Mouchet, M., 1991b, *Ap.J.*, **369**, 490
- Murakami, T., et al. 1988, *Nature*, 335, 234
- Murakami, T., et al. 1991, *Nature*, 350, 592

- Murakami, T., Inoue, H., van Paradijs, J., Fenimore, E., & Yoshida, A., 1992, in *Gamma-Ray Bursts*, ed. C. Ho, R. I. Epstein & E. Fenimore (Cambridge: Cambridge University Press), 239
- Murakami, T., et al., 1998, in *Proceedings of the 4th Huntsville Symposium on Gamma-ray Bursts* AIP Conference Proc. 428, Meegan, C. A., Preece, R. D. & Koshut, T. M. (New York: AIP), 435
- Norris, J.P., Share, G. H., Messina, D. C., Dennis, B. R., Desai, U. D., Cline, T. L., Matz, S. M., & Chupp, E. L., 1986, *ApJ*, 301, 213
- Norris, J.P., Hertz, P., Wood, K. S., & Kouveliotou, C. 1991, *ApJ*, 366, 240
- Paczyński, B. & Kouveliotou, C., 1997, *Nature*, 389, 548
- Pendleton, G. et al. 1996, in *Proc. of the 3rd Huntsville Symposium on Gamma-Ray Bursts AIP Conf. Proc. 384*, ed. C. Kouveliotou, M. F. Briggs, & G. J. Fishman, (New York: AIP) 384
- Pendleton, G. et al., 1997, *ApJ*, 489, 175
- Pilla, R. & Loeb, A., 1997, in *Proc. of the VIII Marcel Grossman Meeting on General Relativity*, eds. R. Ruffini & T. Piran (Singapore: World Scientific) in press
- Piro, L. et al., 1998a, in *Proceedings of the 4th Huntsville Symposium on Gamma-ray Bursts* AIP Conference Proc. 428, Meegan, C. A., Preece, R. D. & Koshut, T. M. (New York: AIP)
- Piro, L., et al., 1997b, *IAU Circ.* 6797
- Piro, L. et al. 1998b; *Bulletin of the American Astronomical Society*, 29, 1303
- Pizzichini, G. 1995, in *Proc. 24th Int. Cosmic-Ray Conf.*, Rome, Italy, 2, 81
- Preece, R. et al., 1996, in *Proc. of the 3rd Huntsville Symposium on Gamma-Ray Bursts AIP Conf. Proc. 384*, ed. C. Kouveliotou, M. F. Briggs, & G. J. Fishman, (New York: AIP) 223
- Press, W. H., Flannery, B. P., Teukolsky, S. A., and Vetterling, W. T., 1986, *Numerical Recipes* (New York: Cambridge University Press)
- Ricker, G. R. et al., 1992, in *Gamma-Ray Bursts: Observations, Analyses and Theories* ed. C. Ho, R. I. Epstein & E. E. Fenimore (Cambridge: Cambridge University Press) 288
- Rothschild, R. *et. al.*, 1979, *SpScInstr*, 4, 269
- Sari, R. & Piran, T., 1996, *MNRAS*, 287, 110
- Scheid, Francis J, 1968, *Schaum's Outline Series of Numerical Methods*, (New York: McGraw-Hill Book Company).
- Smith, D., et al., 1998, in *Proceedings of the 4th Huntsville Symposium on Gamma-ray Bursts* AIP Conference Proc. 428, Meegan, C. A., Preece, R. D. & Koshut, T. M. (New York: AIP), 430
- Strohmayer, T. E., Fenimore, E. E., Murakami, T., & Yoshida, A., 1998, *ApJ* in press.

- Takeshima, Y., et al., 1998, in *Proceedings of the 4th Huntsville Symposium on Gamma-ray Bursts*  
AIP Conference Proc. 428, Meegan, C. A., Preece, R. D. & Kosshut, T. M. (New York:  
AIP), 414
- Tennant, A.F., 1983, *Rapid X-ray Variability of Active Galaxies*, Ph.D. Thesis, University of  
Maryland
- Terrell, J., Fenimore, E. E., Klebesadel, R. W., & Desai, 1982 ApJ, 254, 279
- van Paradijs, J. et al., 1997, Nature, 386, 686
- Vietri, M., 1997, ApJ, 488, L105
- Wheaton, W. A., et al. 1973 ApJ, 185, L57
- Yaqoob, T., 1997, ApJ, 479, 184
- Yoshida, A., et al. 1989, PASJ, 41, 509
- Yoshida, A., Murakami, T., Nishimura, J., Kondo, I, and Fenimore, E. E., 1992, in *Gamma-Ray  
Bursts: Observations, Analyses and Theories*, ed. C. Ho, R. I. Epstein, & E. E. Fenimore,  
(Cambridge: Cambridge University Press), 399

Fig. 1.— *HEAO 1* A–2 HED1 Layer 1 2–20 keV background–subtracted  $\text{cts}\text{-s}^{-1}$  versus time since burst onset (at 82632.97 s U.T.) during the 6 hr point on May 6, 1978. The large gaps are due to Earth occultation; the smaller ones to times of higher particle background.

Fig. 2.— *HEAO 1* A–4 (*top two panels*; in  $\text{cts}/1.28\text{ s}$ ) and A–2 (*middle two panels*; in  $\text{cts}\text{-cm}^{-2}\text{-s}^{-1}$ ) light–curves, and 8–45 keV / 2–6 keV hardness ratio (*bottom panel*) during the burst, in 1.28 s bins. At the top of the figure we have marked the 10.24 s spectra accumulation intervals.

Fig. 3.— *HEAO 1* A–2 (open circles) and A–4  $\nu F_\nu$  spectra, in  $\text{keV}\text{-photons}\text{-cm}^{-2}$  for (a) the first peak of the burst, intervals 1+2; (b) the second peak, intervals 3+4+5; (c) the afterglow.

Fig. 4.— (a)–(f) *HEAO 1* A–2 (open circles) and A–4 spectra, in  $\text{photons}\text{-cm}^{-2}\text{-s}^{-1}\text{-keV}^{-1}$  for each of the six accumulation intervals marked in Figure 3. Except for the first spectrum (Figure 4.a), the *HEAO 1* A–4 data are upper limits. (g) Best–fit spectra for each time interval: 1 (*solid line*), 2 (*dashed line*), 3 (*dot–dashed line*), 4 (*dash–double–dotted line*), and 5 and 6 (*dotted lines*).

Fig. 5.— Background–subtracted 2–20 keV  $\text{cts}\text{-s}^{-1}$  from *HEAO 1* A–2 HED1 Layer 1 (*upper panel*) and *HEAO 1* A–2 HED3 Layer 1 (*lower panel*) showing the faint afterglow immediately following the burst. (The burst itself is off–scale.)

Fig. 6.— *Upper panels*: 95.45% and 99.73% (equivalent to 2 and 3  $\sigma$ ) credible regions for 5 scans of Crab data (*left panel*); and 6 hr of pointed data on the highly variable source GX 301-02 (*right panel*). *Lower panels*: 95.45% and 99.73% (equivalent to 2 and 3  $\sigma$ ) credible regions for 3 hr (*left panel*) and 1 orbit, or about 1 hr (*right panel*) of pointed data on the fainter steady source Abell 401.

Fig. 7.— 95.45% and 99.73% (equivalent to 2 and 3  $\sigma$ ) credible regions for GRB 780506 (*grayscale contours*) plus extended X–ray emission (*line contours*), for data from the (90 minute) orbit containing the burst. Both were calculated using the Bayesian likelihood ratio derived assuming a Gaussian approximation for the direct probability, appropriate for high signal–to–noise data.

Fig. 8.— (*Left panel*) 95.45% and 99.73% (equivalent to 2 and 3  $\sigma$ ) credible regions for 1 orbit (about 1 hr) of *HEAO 1* A–2 MED data of Abell 401. (*Right panel*) the same for the full point (about 3 hr of data).

Fig. 9.— 95.45% and 99.73% (equivalent to 2 and 3  $\sigma$ ) credible regions for GRB 780506 (*grayscale contours*) plus extended X–ray emission (*line contours*), for data from the (90 minute) orbit containing the burst. The latter was calculated using the Bayesian likelihood ratio derived from the full Poisson expression for direct probability, rather than a Gaussian approximation.

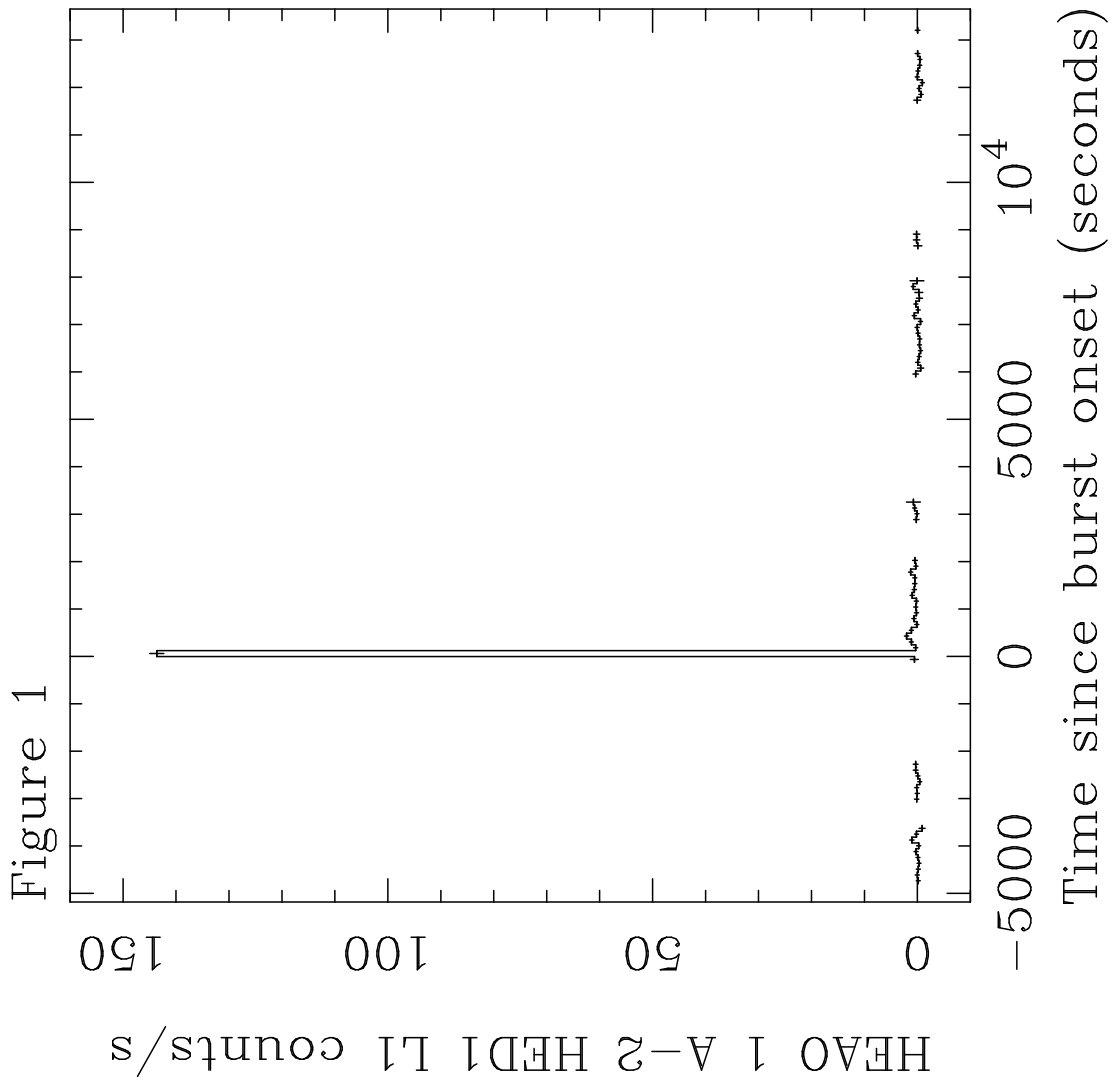


Figure 2

